J|A|C|S
ARTICLES
Published on Web 12/12/2002

# Control of Charge Recombination Dynamics in Dye Sensitized Solar Cells by the Use of Conformally Deposited Metal Oxide Blocking Layers

Emilio Palomares, John N. Clifford, Saif A. Haque, Thierry Lutz, and James R. Durrant*

*Contribution from the Center for Electronic Materials and Devices, Department of Chemistry, Imperial College of Science, Technology, and Medicine, Exhibition Road, London SW7 2AY, United Kingdom*

Received July 31, 2002; E-mail: j.durrant@ic.ac.uk.

***Abstract:*** We report herein a methodology for conformally coating nanocrystalline $TiO_2$ films with a thin overlayer of a second metal oxide. $SiO_2$, $Al_2O_3$, and $ZrO_2$ overlayers were fabricated by dipping mesoporous, nanocrystalline $TiO_2$ films in organic solutions of their respective alkoxides, followed by sintering at 435 °C. These three metal oxide overlayers are shown in all cases to act as barrier layers for interfacial electron transfer processes. However, experimental measurements of film electron density and interfacial charge recombination dynamics under applied negative bias were vary significantly for the overlayers. A good correlation was observed between these observations and the point of zero charge of the different metal oxides. On this basis, it is found that the most basic overlayer coating, $Al_2O_3$ (pzc = 9.2), is optimal for retarding interfacial recombination losses under negative applied bias. These observations show good correlation with current/voltage analyses of dye sensitized solar cell fabricated from these films, with the $Al_2O_3$ resulting in an increase in $V_{oc}$ of up to 50 mV and a 35% improvement in overall device efficiency. These observations are discussed and compared with an alternative $TiCl_4$ posttreatment of nanocrystalline $TiO_2$ films with regard to optimizing device efficiency.

## Introduction

Control of the structure of inorganic materials on the nanometer scale is currently attracting extensive interest. A range of fabrication procedures have been developed for the fabrication of mesoporous, nanocrystalline metal oxide films comprising continuous networks of inorganic nanoparticles with dimensions ranging from 5 to 200 nm. Such films are now attracting interest as electrodes for solar cells,[1] smart windows,[2] displays, bio-inorganic applications,[3] and heterosupramolecular devices.[4,5] Interfacial electron-transfer dynamics are fundamental to all of these device applications. Optimization of these interfacial dynamics, and specifically the development of film structures that minimize interfacial recombination dynamics relative to charge transport through the film, is a key issue in achieving improvements in device performance. Research into this area is increasingly addressing the use of sol−gel chemistry procedures to obtain more sophisticated architectures and thereby improved function.[6,7] It has recently been suggested that the conformal growth of insulating overlayers on the surfaces of such nanoporous films may be an important approach to achieve this.[8−11] In this paper, we address in detail the growth of conformal metal oxide insulating overlayers on preformed nanocrystalline $TiO_2$ films, focusing on the ability of such insulating layers to retard interfacial recombination dynamics and thereby modulate the performance of Dye Sensitized Solar Cells fabricated from these films.

Dye sensitized solar cells[12] (DSSC) comprises a dye sensitized nanocrystalline porous metal oxide film, interpenetrated by a hole transporting material, typically a liquid electrolyte containing an $I^-/I^-_3$ red/ox couple.[13] The main charge-transfer events taking place at the $TiO_2$/dye/electrolyte interface are depicted in Scheme 1. Visible light is absorbed (**d**) by the sensitizer dye (e.g., $RuL_2(NCS)_2$ where L is 4,4′-dicarboxy-2,2′-bipyridyl) followed by electron injection (**b**), from the excited state of the dye into the conduction band of the $TiO_2$. The dye ground state is then regenerated by electron transfer from an $I^-/I_3^-$ redox couple in film pores (**e**). Efficient operation of the DSSC devices

(1) O'Regan, B.; Grätzel, M. *Nature* **1991**, *353*, 737−739.
(2) Janez, K.; Marko, T.; Smole, F.; Krasovec, O.; S., L. U.; Orel, B. *Sol. Energy. Mater. Sol Cells* **2002**, *71*, 387−395.
(3) Topoglidis, E.; Collin, J. C.; Palomares, E.; Durrant, J. R. *Chem. Commun.* **2002**, 1518−1519.
(4) Ryan, D.; Rao, S. N.; Rensmo, H.; Fitzmaurice, D.; Preece, J. A.; Wenger, S.; Stoddart, J. F.; Zaccheroni, N. *J. Am. Chem. Soc.* **2000**, *122*, 6252−6257.
(5) Cusack, L.; Marguerettaz, X.; Rao, S. N.; Nagaraja, S.; Wenger, J.; Fitzmaurice, D. *Chem. Mater.* **1997**, *9*, 1765−1772.
(6) Decher, G. *Science* **1997**, *277*, 1232.
(7) Caruso, R. A.; Susha, A.; Caruso, F. *Chem. Mater.* **2001**, *13*, 247−279.
(8) Tennakone, K.; Bandara, J.; Bandaranayake, P. K. M.; Kumara, G. R. R. A.; Konno, A. *Jpn. J. Appl. Phys.* **2001**, *40*, L732−L734.
(9) Kumara, G. R. R. A.; Tennakone, K.; Perera, V. P. S.; Konno, A.; Kaneko, S.; Okuya, M. *J. Phys. D: Appl. Phys.* **2001**, *34*, 868−873.
(10) Zaban, A.; Chen, S. G.; Chappel, S.; Gregg, B. A. *Chem. Commun.* **2000**, 2231.
(11) Palomares, E.; Clifford, J. N.; Haque, S. A.; Lutz, T.; Durrant, J. R. *Chem. Commun.* **2002**, 1464−1465.
(12) Gratzel, M. *Nature* **2001**, *414*, 338−344.
(13) Hagfeldt, A.; Graetzel, M. *Acc. Chem. Res.* **2000**, *33*, 269−277.

10.1021/ja027945w CCC: $25.00 

***Scheme 1.*** Schematic Representation of Electron Transfer Processes in Dye-Sensitized Blocking-Layer Photoelectrode Showing Photogeneration of the Dye Excited State (d), Electron Injection into the Conduction Band of Nanoporous TiO2 (b), Regeneration of the Dye Ground State by Electron Transfer from the Redox Couple (e), and the Wasteful Charge Recombination Pathways of Injected Electron Recombination Oxidized Dye Molecules (c) and with Oxidized Redox Couple (f). Also Shown Is Dye Excited State Decay to Ground (a), Which Competes with Electron Injection

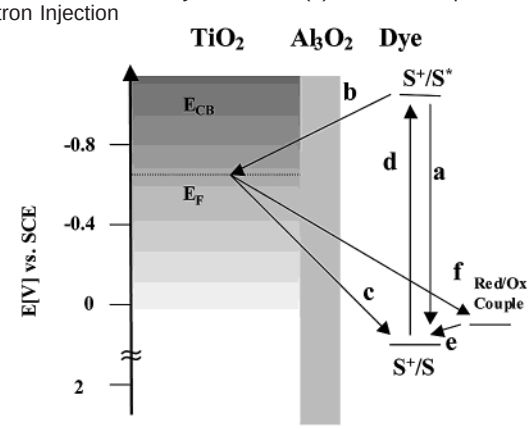


relies upon the minimization of the possible recombination pathways occurring at the $TiO_2$/dye/electrolyte interface,[14] allowing efficient charge transport through the $TiO_2$ film and the electrolyte and subsequent charge collection at the device contacts. Two interfacial recombination pathways are of primary importance for DSSC's: the injected electrons may recombine either with oxidized dye molecules (**c**) or with the oxidized redox couple (**f**). The latter is thought to be particularly critical to device function.[15]

In the last two years, several groups, including our own, have demonstrated procedures for conformally coating nanocrystalline metal oxide films with a thin overcoat of a different metal oxide with a higher conduction band edge,[11,16,17] as illustrated in Scheme 1. This overcoat is intended to increase the physical separation of injected electrons and oxidized dyes/ red-ox couple and thereby retarding the recombination reactions.[18] Such conformal coating films are analogous to binary core/shell nanoparticles, where electronically insulating shell layers are grown on nanoparticles in solution to shield the core material of the nanoparticle from the external environment.[19] We note however that for the DSSC, it is preferable that the coating is conducted conformally upon the preformed metal oxide film; the fabrication of films from precoated core/shell nanoparticles, as has been employed in several recent reports,[16,18,20,21] can be expected to result in insulating barriers between the nanoparticles, impeding efficient electron transport through the film. Studies to date have demonstrated improvements in DSSC device performance for $Nb_2O_5$ coated $TiO_2$ films and for films fabricated from $SnO_2$ particles coated with MgO [8]and ZnO.[22]

***Table 1.*** Characteristics of the Metal Oxides Employed in This Study

| metal oxide | band-gap [eV] | $E_{VB}$ [V vs SCE][b] | $E_{CB}$ [V vs SCE][a] | Pzc (pH units) |
|---|---|---|---|---|
| $SiO_2$ | 8−8.9 | +4.01 | −4.48 | 2.1 |
| $ZrO_2$ | 5.0 | +3.75 | −1.24 | 5.1 |
| $Al_2O_3$ | 8.45−9.9 | +3.85 | −4.45 | 9.2 |
| $TiO_2$ | 3.0−3.3 | +2.73 | −0.42 | 5.5 |

[a] For comparison the thermalized excited-state oxidation potential of the sensitizer dye $RuL_2(NCS)_2$ is +0.84V vs SCE. [b] For comparison with potentials versus Ag/AgCl, V vs SCE is equivalent to −0.039 V at 25 °C versus Ag/AgCl.

Building upon these studies, we have recently reported a rather simple procedure for the fabrication of an $Al_2O_3$ coated $TiO_2$ film,[11] and demonstrated that this coating resulted in both retardation of interfacial recombination dynamics and improvement in device performance.

In this paper, we compare the function of three different metal oxide overcoats, $Al_2O_3$, $ZrO_2$, and $SiO_2$, grown on preformed nanocrystalline $TiO_2$ semiconductor films. We consider the ability of these films to modulate interfacial electron transfer dynamics and thereby improve the performance of DSSCs. The key materials properties of these metal oxides are summarized in Table 1. It is apparent that the conduction band edge for all three metal oxides are significantly negative of both the $TiO_2$ conduction band edge and dye excited state oxidation potential, indicating that all three metal oxides should function as physical barrier layers for both electron injection and charge electron recombination reactions. We note, however, that these metal oxides differ significantly in their point of zero charge (Pzc). We show herein that there is a strong correlation between the pzc of these metal oxides, and the ability of overcoats fabricated from these metal oxides to improve the performance of dye sensitized solar cells.

## Experimental Section

Silicon Methoxide (99.9%) Alumina tri *sec*-buthoxide (99.9%), Zirconia iso-butoxide (99.9%) and the remaining chemicals s were purchased from Aldrich Chemical Co. and used as received, except Carbowax 20,000(Fluka). The dye $RuL_2(NCS)_2$ (chemical name [cis-bis(isothiocyanato) bis(2,2′-bipyridyl-4,4′-dicarboxylato)-ruthenium(II) bis-tetrabutylammonium] was received from Johnson Matthey Ltd. Conducting glass substrates (15 Ohm/square F-doped $SnO_2$) were cleaned with water, rinsed with ethanol, dried at 100 °C in the oven and fired prior to film deposition.

The thickness of the nanocrystalline $TiO_2$ films was measured with a DEKTAK profilometer. Absorption spectra were recorded using a Shimadzu 1601 UV−vis. Spectrometer. High-Resolution Transmission Electron Microscopy (TOPCON 002B 200keV) was employed to determine overcoat thickness and estimate the average particle size. X-ray Photoelectron Spectroscopy (XPS) measurements were employed to determine film composition from the relative intensities of the Ti 3p, Al 2p, and Si 2p signals.

The $TiO_2$ paste, consisting of 15 nm sized particles as determined by HRTEM, were prepared from a sol−gel colloidal suspension containing 12.5wt % $TiO_2$ particles and 6.2wt % Carbowax 20 000. The nanoparticles were fabricated by the following procedure. 20 mL of titanium iso-propoxide were injected into 5.5 g. of glacial acetic acid under argon atmosphere and stirred for 10 min. The mixture was then injected into 120 mL of 0.1 M nitric acid under anhydrous atmosphere at room temperature in a conical flask and stirred

(14) Kalyanasundaram, K.; Gratzel, M. *Micelles, Microemulsions, Monolayers, Int. Symp.* **1998**, 579−603.
(15) Kebede, Z.; Lindquist, S.-E. *Sol. Energy. Mater. Sol Cells* **1999**, *57*, 259.
(16) Kumara, G. R. A.; Konno, A.; Tennakone, K. *Chem. Lett.* **2001**, 180−181.
(17) Zaban, A.; Chen, S.; Sukenik, C. N.; Pizem, H. *Abstracts of Papers, 222nd ACS National Meeting, Chicago, IL, United States, August 26−30, 2001* **2001**, CHED-285.
(18) Tennakone, K.; Bandara, J.; Bandaranayake, P. K. M.; Kumara, G. R. A.; Konno, A. *Japn. J. Appl. Phys., Part 2: Lett.* **2001**, *40*, L732−L734.
(19) W., C. Y.; Banin, U. *Angew. Chem., Int. Ed. Engl.* **1999**, *38*, 3692−3694.
(20) Kumara, G.; Tennakone, K.; Perera, V. P. S.; Konno, A.; Kaneko, S.; Okuya, M. *J. Phys. D-Appl. Phys.* **2001**, *34*, 868−873.
(21) Chappel, S.; Chen, S. G.; Zaban, A. *Langmuir* **2002**, *18*, 3336−3342.
(22) Kumara, G. R. R. A.; Konno, A.; Tennakone, K. *Chem. Lett.* **2001**, *2*, 180−181.

vigorously. The flask was left uncovered and heated at 80 °C for 8 h. After cooling, the solution was filtered using a 0.45 mm syringe filter, diluted to 5wt % $TiO_2$ by the addition of $H_2O$ and then autoclaved at 220 °C for 12 h. The colloids were re-dispersed with a 60 s cycle burst from a LDU Soniprobe horn as reported before,[14] the solution was then concentrated to 12.5% on a rotary evaporator using a membrane vacuum pump at a temperature at 40 °C. 6.2 wt %. Carbowax 20 000 was added and the resulting paste was stirred slowly overnight to ensure homogeneity. The suspension was spread on the substrates by a glass rod, using 3M adhesive tapes as spacers. After the films were dried in air, they were sintered at 450 °C for 20 min in air. The thickness of the $TiO_2$ films was controlled using different tapes, resulting in film thicknesses of between 4 and 8 mm.

After sintering, the $TiO_2$ films were coated with metal oxides overlayers by dipping each film in a solution of suitable precursors, followed by sintering at 435 °C for 20 min, following a methodology based on the hydroxylation of the $TiO_2$ films as described previously.[23] The precursor solutions employed were 0.15 M solution of aluminum tri-*sec*-butoxide in dry 2-propanol, 0.15 M of silicon methoxide in dry methanol and 0.15 M solution of zirconium iso-butoxide. These nonscattering precursor solutions were prepared under anaerobic conditions in a glovebox; however, once prepared the solutions were not air sensitive, allowing dipping to be conducted under ambient conditions. To keep similar conditions between the standard and coated electrodes, the nanoporous $TiO_2$ films without coatings were sintered at the same time as coated ones. The precursor solution was heated to 60−70 °C prior to dipping the nanocrystalline film in the solution for 20 min. Experiments were conducted as a function of precursor concentration, dipping time and temperature and repeated dipping/sintering cycles. The overlayer growth was found to be insensitive to dipping time or temperature, but dependent upon precursor concentration and the number of repeat cycles, consistent with previous observations.[23] For convenience, the precursor concentration was maintained at 0.15 M for all studies reported in this paper, with overlayer thickness being controlled only by repeating the dipping/sintering cycle up to 4 times.

Sensitization of the photoelectrodes with $RuL_2(NCS)_2$ was achieved by immersing the electrodes in a 1mM solution of dye in 1:1 acetonitrile/*tert*-butyl alcohol overnight, followed by rinsing in ethanol to remove unadsorbed dye.

**Nanosecond-Millisecond Laser Transmittance Spectroscopy.** Transient absorption studies of the dye sensitized nanocrystalline films were conducted as detailed previously by covering the film with a 1:1 ethylene carbonate/propylene carbonate solution and glass cover slide.[24] For determination of the transient absorption data, samples were excited at 625 nm with pulses from a nitrogen laser pumped dye laser (<1ns pulse duration, 0.8 Hz, intensity ~0.04 mJ $cm^{-2}$). The optical density of the dye sensitized films at 625 nm was ~0.3 resulting in 0.5−1 absorbed photon per nanoparticle. The resulting photoinduced change in optical density was monitored by employing a 100 W Tungsten lamp, with 20 nm bandwidth monochromators before and after sample, a home-built photodiode based detection system and a TDS-220 Tecktronic DSO oscilloscope. UV−vis measurements were performed after each experiment to monitor any desorption/degradation of the sensitizer dye. No changes in the UV−vis spectra were observed for the photoelectrodes after transient absorption experiments.

For the experiments under external applied bias, the dye-sensitized nanoporous metal oxide film formed the working electrode (~1 $cm^2$ macroscopic surface area) in a three-electrode photoelectrochemical cell employing a platinum foil counter electrode and a Ag/AgCl reference electrode. The electrolyte solution comprised 0.1 M tetra butylammonium perchlorate, 0.1M $LiClO_4$ in 15 mL anhydrous acetonitrile, prepared with a final water content of <20 ppm $H_2O$ determined by a Metrohm 737 Coulometer. The solution was degassed with argon gas prior to and during all optical experiments. The effect of applied bias upon transient data was reversible in all cases.

**Potential Step Chronoamperometry.** Chronoamperometry studies employed the three-electrode cell as detailed above, except that the films were unsensitized. The three-electrode cell was left at + 200mV vs Ag/AgCl reference for 10 min to allow equilibrium to be reach. A bias step of −25 mV was then applied, the current transient recorded (~50 k samples/sec) and integrated as detailed below. The same procedure was carried out at 100mV intervals, with the sample held at the new voltage for 5 min prior each −25 mV step to allow stabilization of the dark current. Electron flow into the film was quantified by integration of the fast charging transient observed following each potential step, yielding a potential dependent film capacitance. Slow charging transients, most probably associated with lithium diffusion/intercalation processes, were neglected as discussed previously.[25] Integration of these film capacitances allowed calculation of the density of electrons added to the film as function of the applied bias.

**Photovoltaic Device Characterization.** The dye-sensitized films were cut up into smaller electrodes with an active area of 0.8 $cm^2$ and were stored under a dry atmosphere. A sandwich cell was prepared with a second conducting glass coated with chemically deposited platinum from 0.05 M hexachloroplatinic acid (Aldrich) in 2-propanol (Aldrich). Both titanium dioxide and platinum plates were then sealed together with a transparent film of Surlyn 1472 polymer (DuPont) at 110 °C. The electrolyte comprised Tetra-butylammonium iodide 0.6M (2.216 g), LiI 0.1M (0.134 g), $I_2$ 0.1M (0.253 g), and 4-*tert*-butyl pyridine 0.5M (0.676 g) in 10 mL. This electrolyte was introduced through holes drilled in the counter electrode, which were sealed immediately with a microscope cover slide and additional Surlyn to avoid leakage of the electrolyte solution. Current/voltage measurements were made with a ScienceTech solar simulator and AM1.5 spectral filter. Calibration of the light intensity was achieved using band-pass filters of know transmission combined with a silicon photodiode with independently certified spectral response. The lamp intensity was adjusted to give a close (± 5%) agreement with the theoretical AM 1.5 intensity over the spectral region of dye optical absorption (450−700 nm).

## Results

**Materials Characterization.** HRTEM was employed to investigate the thickness and uniformity of the overlayers grown on nanocrystalline $TiO_2$ films as detailed above. Following film fabrication and overlayer growth, the films were removed from the glass substrate, powdered, and then deposited on the TEM grid. Data are shown in Figure 1, comparing data for an uncoated film (Figure 1c and 1d) with data obtained for a film coated with a single layer of $Al_2O_3$ (Figure 1a and 1b). The $Al_2O_3$ overlayer is clearly visible, conformally coating all of the particles, with a film thickness of 900 ± 100 Å. Overcoat thicknesses were furthermore investigated by XPS measurements. For single overlayers, peak ratios for Ti:Al ratio of 1.7:1 and for Ti:Si of 1.5:1, indicative of film thicknesses of between 0.7 and 1 nm, assuming a homogeneous coating thickness[10,21]-consistent with the HRTEM data.

Nitrogen absorption analysis indicted the pore volume fraction of the films was unaffected by the coating procedure (at least for single overlayers), with an effective surface of 147 $m^2/g$ being obtained for all films. Pore volume fractions, determined from the mean film density by weighing a know volume of film, were also found to be unaffected by the single overlayer, being in all cases 40 ± 5%.

(23) Ichinose, I.; Senzu, H.; Kunitake, T. *Chem. Mater.* **1997**, *9*, 1296−1298.
(24) Haque, S. A.; Tachibana, Y.; Willis, R. L.; Moser, J. E.; Graetzel, M.; Klug, D. R.; Durrant, J. R. *J. Phys. Chem. B* **2000**, *104*, 538−547.
(25) Willis, R. L.; Olson, C.; O'Regan, B.; Lutz, T.; Nelson, J.; Durrant, J. R. *J. Phys. Chem. B* **2002**, In press.

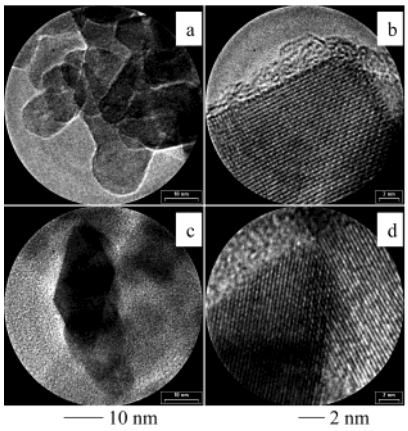


***Figure 1.*** HRTEMs of $TiO_2$ nanoparticles in the presence (a, b) and absence (c,d) of an $Al_2O_3$ overlayer. The $Al_2O_3$ overlayer was grown conformally on a preformed nanocrystalline $TiO_2$. This film, and the uncoated control, was then broken up to a powder to allow HRTEM analysis. Pictures (b) and (d) are at high magnification.

Dye adsorption was monitored by collecting UV−vis absorption spectra of the films before and after immersion in the sensitizing solution. The spectra were not corrected for film scatter, however the films employed were all nonscattering (optical transmission > 95% for wavelength > 415 nm). Single or double overlayer growth did not increase sample scatter; however, further repeat coatings resulted in a significant increase in film optical scatter. The overlayer treatment was found to result in a ∼2-fold retardation of the time for dye adsorption for all three metal oxide overlayers; in all cases, however, overnight sensitization resulted in saturation of dye adsorption. This sensitization resulted in film optical densities of 1.6 and 2.2 and 0.8 absorbance units in noncoated nanocrystalline $TiO_2$ and coated photoelectrodes with alumina and silica films respectively (optical density monitored at 535 nm, the $RuL_2(NCS)_2$ absorption maximum). It is apparent from these data that the overlayer with the highest pzc, and therefore, the most basic film surface, resulted in the highest dye adsorption, as has been observed previously for metal oxide coated $SnO_2$ films.[26]

**Electron Recombination Kinetics.** The primary function of the overlayer deposition is to retard interfacial charge recombination (reactions **c** and **f** in Scheme 1). We employed transient absorption spectroscopy to assay this function, monitoring the decay of induced absorption of the $RuL_2(NCS)_2$ cation due to reaction **c** observed following pulsed laser excitation of the sensitized films in the absence of any applied bias or redox active electrolyte. As shown in Figure 2, $ZrO_2$, $Al_2O_3$, and $SiO_2$ overlayers all result in significant retardation of the recombination dynamics, consistent with the expected blocking layer function of these materials. It is furthermore apparent that the electron injection yield (reaction 2), monitored by the initial amplitude of the cation absorption signal, is essential unaffected by these overlayers.

Figure 3 addresses the influence of overlayer thickness on the interfacial electron-transfer dynamics. Data are shown for $TiO_2$ films following either one (as in Figure 2) or two immersions in Alumina tri *sec*-buthoxide solution. It is apparent that the recombination dynamics are further retarded by the repeat dipping, consistent with increased thickness of the $Al_2O_3$ overlayer. However, this repeat immersion results in a loss of the initial dye cation signal, indicating that thicker overlayers results in a retardation of the electron injection dynamics to such an extent that they no longer compete successfully with dye excited-state decay. For this reason, for the remainder of this paper we focus on overlayer coatings fabricated by a single immersion procedure, as employed in Figure 2. A more detailed analysis of the influence of overlayer thickness upon injection dynamics will be presented elsewhere.

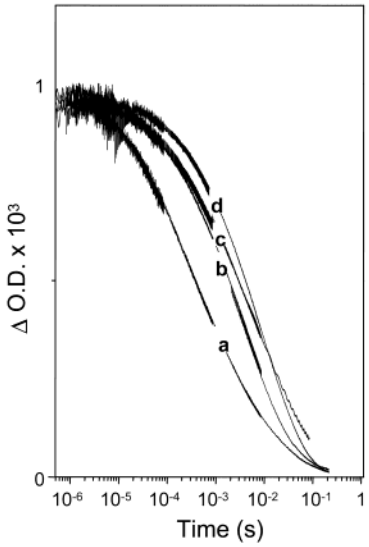


***Figure 2.*** Transient absorption data monitoring photoinduced absorption of the $RuL_2(NCS)_2$ cation following optical excitation of the dye adsorbed on nanoporous (a) $TiO_2$, (b) $Al_2O_3/TiO_2$, (c) $SiO_2/TiO_2$, and (d) $ZrO_2/TiO_2$ photoelectrodes. The signal decay is assigned to charge recombination of the dye cation with electrons in trap/conduction band states of the $TiO_2$ semiconductor (reaction c in Scheme 1). Optical excitation is at 630 nm, and detection at 800 nm.

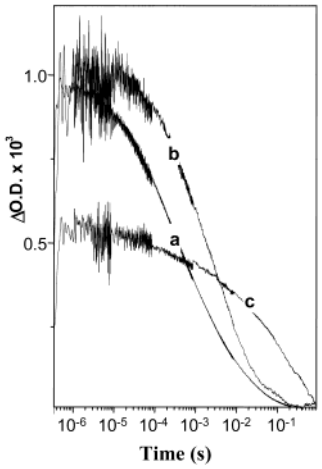


***Figure 3.*** Transient absorption data monitoring photoinduced absorption of the dye cation following optical excitation of the dye $RuL_2(NCS)_2$ adsorbed on nanocrystalline $TiO_2$ films with (a) 0, (b) 1, and (c) 2 $Al_2O_3$ overlayer coatings.

**Influence of Applied Bias.** Interfacial recombination dynamics in dye sensitized nanocrystalline $TiO_2$ films are strongly dependent upon the electron density *n* in, and therefore the Fermi level of, the metal oxide film. This dependence is critical to the function of DSSCs, as electron injection into the metal oxide film under illumination results in a significant electron density in conduction band/trap states of $TiO_2$ film, and is indeed integral to generation of a photovoltage in such devices.

(26) Kay, A.; Grätzel, M. *Chem. Mater.* **2002**, *14*, 2930−2935.

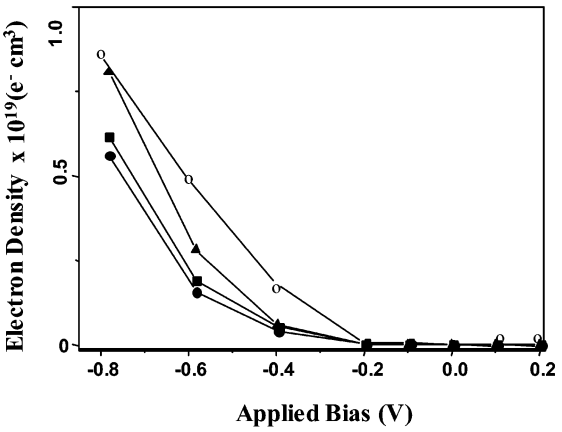


***Figure 4.*** Electron densities *n* added to the nanocrystalline films by an applied external bias(Ag/AgCl electrode reference) in a three electrode cell with redox inactive electrolyte, determined from integration of film capacitances obtained by integration of potential step chronoamperometry data. Data shown for (■) $TiO_2$, (○) $SiO_2/TiO_2$, (▲) $ZrO_2/TiO_2$, and (●) $Al_2O_3/TiO_2$ films.

The function of overlayer coated films under applied bias was investigated by incorporating the films as the working electrode of a three electrode photoelectrochemical cell. Electron occupancies as function of applied bias were determined by potential step chronoamperometry and correlated with transient absorption measurements of interfacial recombination dynamics. The potential step technique is summarized in the Materials and Methods and reported in more detail elsewhere.[25] Electron densities *n* determined by this technique for unsensitized films are shown in Figure 4. It is apparent that the bias dependence of the electron densities is strongly dependent upon the metal oxide overlayer. Although $Al_2O_3$ overlayer results in a reduced dependence of *n* upon applied bias, both $SiO_2$ and $ZrO_2$ overlayer result in an increase this dependence relative to the uncoated $TiO_2$ film. Qualitatively similar results were obtained from cyclic voltametry, with film charging under negative potentials being observed to be greatest for $SiO_2$ coated films, and least for $Al_2O_3$ coated films.

Figure 5 addresses the bias dependence of the interfacial recombination dynamics as function of metal oxide overlayer. Transient absorption data such as those shown in Figure 2 were collected as a function of applied bias. The half times for these decays, $t_{50\%}$, are plotted in Figure 5 as a function of the applied bias. At positive applied biases, when the film electron densities are expected to be dominated by electrons photoinjected by the pulsed laser excitation, and therefore, independent of overlayer composition, both the $Al_2O_3$ and $SiO_2$ overlayers result in a ~4-fold increase in $t_{50\%}$ relative to the control films with no overlayer. This retardation of the recombination dynamics is in agreement with the recombination data obtained in the absence of applied bias shown in Figure 2. However, under negative applied biases, the recombination dynamics exhibit remarkably different dependencies upon applied bias depending for the two different metal oxide overlayers. For the $SiO_2$ coated films, the recombination dynamics accelerate rapidly at negative biases, and for biases $< -300$ mV are actually faster than for the uncoated nanoporous $TiO_2$ film. In sharp contrast, for the $Al_2O_3$ oxide coated film, the recombination dynamics are almost independent of applied potential for voltages up to −800mV.

It can be concluded from the above that the $Al_2O_3$ overlayer is most effective at retarding the interfacial charge recombination, reaction **c** in Scheme 1. This effect is largest at negative applied biases, an observation of particular importance as such applied potentials correspond to the Fermi levels expected in devices operating load.

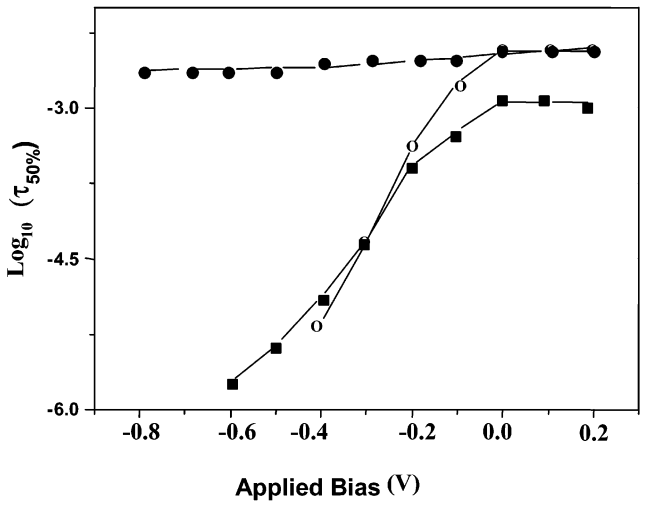


***Figure 5.*** Dependence of the half time for charge recombination $t_{50\%}$ upon applied bias (Ag/AgCl electrode reference) for $RuL_2(NCS)_2$ sensitized (■) $TiO_2$, (**O**) $SiO_2/TiO_2$ and (●) $Al_2O_3/TiO_2$ films. $t_{50\%}$ data obtained from transient absorption decays analogous to those shown in Figure 2 collected as a function of applied bias in a three electrode photoelectrochemical cell with redox inactive electrolyte.

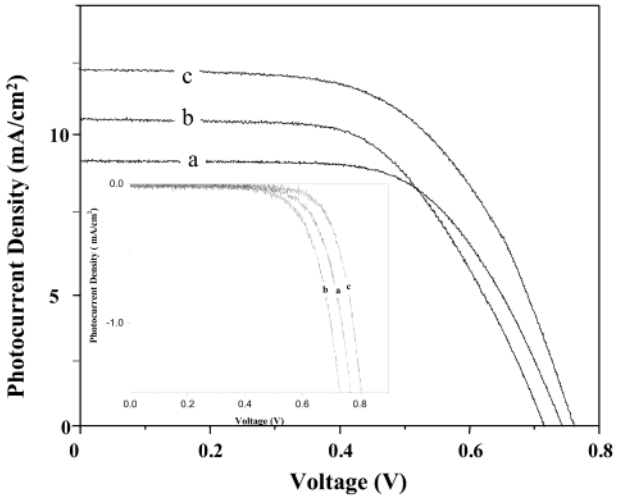


***Figure 6.*** Current/voltage characterizitics of typical dye sensitized solar cells fabricated employing $RuL_2(NCS)_2$ sensitized (a) $TiO_2$, (b) $SiO_2/TiO_2$, and (c) $Al_2O_3/TiO_2$ films. Data are shown for film thicknesses were 8 mm, cell active areas were 0.8 $cm^2$. Data shown were obtained under AM1.5 simulated sunlight, ~100 $mWcm^{-2}$ calibrated as detailed in Materials and Methods. The insert shows the corresponding dark current data. All data obtained for nonscattering films with transparent counter electrodes.

**Dye Sensitized Solar Cells.** The photovoltaic performance of the DSSC nanocrystalline films were assessed by the fabrication of "sandwich" type DSSCs. The sensitization time of the films were adjusted to ensure equal dye loadings for all photoelectrodes, to avoid differences in device performance deriving only from differences in dye loadings between the different films. Typical data obtained in the dark and under AM 1.5 simulated solar irradiance are shown in Figure 6. The dark current data address the voltage dependence of the recombination reaction to oxidized redox species in the electrolyte (reaction **e** in Scheme 1). It is apparent that the voltage dependence of

***Table 2.*** Current/Voltage Characteristics of Dye Sensitized Solar Cells Fabricated from Coated and Uncoated $TiO_2$ Films Sensitized with $RuL_2(NCS)_2$ and Obtained under AM1.5 Simulated Sunlight[b]

| | $h$ (%)[e] | $V_{OC}$ (mV) | $J_{SC}$ (mA/cm$^2$) | ff (%) |
|---|---|---|---|---|
| [a]$TiO_2$ | 3.7 | 735 | 9.1 | 55.1 |
| [a]$SiO_2/TiO_2$ | 4.4 | 710 | 10.6 | 58.1 |
| [a]$Al_2O_3/TiO_2$ | 5.6 | 760 | 12.1 | 61.1 |
| [a,c]$Al_2O_3/TiO_2$ | 1.4 | 860 | 2.45 | 65.6 |
| [a]$ZrO_2/TiO_2$ | 3.6 | 675 | 9.1 | 59.5 |
| [d]$TiO_2$ | 2.0 | 710 | 5 | 54.4 |
| [d]$SiO_2/TiO_2$ | 2.3 | 710 | 5.1 | 58.3 |
| [d]$Al_2O_3/TiO_2$ | 2.5 | 760 | 5 | 65.4 |
| [d]$ZrO_2/TiO_2$ | 2.0 | 710 | 5.1 | 51.6 |

[a] 8 mm thickness film. [b] Data presented here were collected with nonscattering films and matched dye loading (approximately ~80% monolayer coverage) in order to focus on the influence of the coating on the interfacial dynamics, as detailed in the text. The use of scattering films and saturated dye loading (EP, JRD, Md. Nazeeruddin, and M. Grätzel, unpublished data) resulted in average device efficiencies of 6% and 6.9% for $TiO_2$ and $Al_2O_3/TiO_2$ films, respectively. [c] $Al_2O_3$ overlayer coated four times. All other data for single overlayer coatings [d] 4 mm thickness film. [e] All data presented are average data obtained from a minimum of 7 devices for each film type, with all devices fabricated from a single batch of $TiO_2$ paste.

the dark current is enhanced by the $SiO_2$ overlayer but reduced by the $Al_2O_3$ overlayer, in good agreement with the voltage dependence of the $t_{50\%}$ data shown in Figure 5 for recombination to dye cations (reaction (**c**) in Scheme 1).

Device performance characteristics under simulated sunlight are summarized in Table 2. As expected from the recombination data presented above, devices fabricated from $Al_2O_3/TiO_2$ exhibit the best device performance, with an increase of open circuit voltage of ~50 mV relative to the uncoated film, and an increase in the fill factor. A similar result was obtained for devices fabricated for optimum device efficiency (i.e., saturated rather than matched dye loadings, scattering rather than transparent electrode) which yielded average device efficiencies of 6% and 6.9% for $TiO_2$ and $Al_2O_3/TiO_2$ films respectively (EP, JRD, Md. Nazeeruddin and M. Grätzel, unpublished data). It is furthermore apparent from the data in Table 2 that there is a good correlation between the shift in the voltage dependence of the dark current and $V_{oc}$ for the different films, consistent with recombination reaction **e** being the primary loss mechanism in the device illumination.

Table 2 shows data obtained for devices fabricated both from 4 and 8 mm $TiO_2$ films. It is apparent that for the 8 mm films, all three metal oxide overlayers result in an enhancement in $I_{sc}$. This increase in $I_{sc}$ was not observed for devices fabricated from 4 mm films. Furthermore, as indicated in Table 2, the use of a thicker $Al_2O_3$ overlayer results in a further increase in $V_{oc}$, but at the expense of a lower $I_{sc}$ and lower overall device power efficiency, consistent with the transient data shown in Figure 3.

## Discussion

In this paper, we have investigated the effect of conformal insulating layers grown on nanocrystalline $TiO_2$ films on their interfacial electron dynamics, and thereby on the performance of dye sensitized solar cells fabricated from these films. The insulating layers employed, $Al_2O_3$, $SiO_2$, and $ZrO_2$, are expected to act as barrier layers for all of the interfacial electron transfer reactions detailed in Scheme 1 (reactions b, c, and f). The central rational for this approach is that device efficiency is critically dependent upon retardation of interfacial charge recombination losses, but less dependent upon the interfacial injection dynamics. The latter rationale is based upon the observation that the injection reaction for uncoated films is much faster than the dye excited-state decay to ground. For the di-TBA salt of $RuL_2(NCS)_2$ employed in this study, we have previously reported the half time for electron injection to be ~12 ps,[27] approximately 100 faster than dye excited state decay in the absence of electron injection, suggesting that the injection yield will be insensitive to a modest retardation of the rate of electron injection. The former rational is based upon the widely accepted concept that charge collection in DSSCs is largely limited by kinetic competition between charge transport in the $TiO_2$ film and/or electrolyte and interfacial charge recombination. This kinetic competition is expected to be particularly critical when operating the cell under load, as under these conditions the electron density in the film is highest, and therefore the recombination dynamics most critical.

We have demonstrated that conformal overlayers of a range of metal oxides can be grown on porous nanocrystalline $TiO_2$ films by a solution chemistry approach under aerobic conditions. The overlayer thickness, may be controlled by repeated dipping. The chemical mechanism of this overlayer growth has been discussed previously[28] for the growth of different metal alkoxides such as $Ti(iOPr)_4$ layers on conducting glass substrates. The coating procedure route is based on an in situ polymerization reaction initiated by hydroxyl groups on the hydrated $TiO_2$ surface, leading to the hydrolysis and condensation of metal alkoxides precursors. Sintering at 430 °C completes polymerization process started by the physi-adsorbed water on nanocrystalline $TiO_2$ film.

Our studies have investigated three different metal oxide overlayers on $TiO_2$:$Al_2O_3$, $SiO_2$, and $ZrO_2$. In all cases, a retardation of interfacial recombination dynamics in observed, consistent with the blocking layer function of these overlayers. For the case of $Al_2O_3$, we have studied the influence of layer thickness and observe that as expected, the recombination half time increases with overlayer thickness. The HRTEM data of coated nanoparticles (Figure 1) indicate a reasonably homogeneous overlayer thickness. This observation is consistent with the recombination data shown in Figure 2. An inhomogeneous overcoat thickness would result in more dispersive (i.e., more stretched) recombination kinetics, whereas we observe the coating actually results in less dispersive (i.e., more monoexponential) kinetics, indicative of a homogeneous film thickness. The small reduction in the dispersion of the kinetics with the overcoats is attributed to a shift from transport to interface limited recombination dynamics, as we have discussed elsewhere.[29] We note that multiple overlayer coatings result in more dispersive recombination dynamics (Figure 3) and (for >2 coatings) more optically scattering films, indicating that overlayer thickness becomes less homogeneous with such multiple treatments.

All three metal oxide overlayers result in similar retardation of the recombination dynamics in the absence of applied bias; however their influence on the recombination dynamics under applied biases are remarkably different, as illustrated in Figure

(27) Tachibana, Y.; Nazeeruddin, M.; Grätzel, M.; Klug, D. R.; Durrant, J. R. *Chem. Phys.* **2002**, *285*, 127−132.
(28) Ichinose, I.; Kawakami, T.; Kunitake, T. *Adv. Mater.* **1998**, *10*, 535−539.
(29) Clifford, J. N.; Yahioglu, G.; Milgrom, L. R.; Durrant, J. R. *Chem. Commun.* **2002**, 1260−1261.

5. We have previously demonstrated that the dependence of the recombination dynamics upon applied bias derives from the influence of the applied bias upon the density of electrons in conduction band/sub band gap states of the $TiO_2$ film $n(V)$. Our previous studies[24,30] have demonstrated a strong correlation between $n(V)$ and bias dependence of recombination half time $t_{50\%}(V)$ for both nanocrystalline $TiO_2$ and ZnO films. Comparison of Figures 4 and 5 shows there is clear correlation between the chronoamperometric and transient absorption data for the different films. The $Al_2O_3$ coated film exhibits the smallest dependence of both $n$ and $t_{50\%}$ upon bias. The $SiO_2$ and $ZrO_2$ coated films exhibit the strongest dependence of both $n$ and $t_{50\%}$ upon bias; for the $SiO_2$ coated film this bias dependence is so great that for biases $<-300$ mV, the recombination dynamics are faster than for the uncoated film.

The influence of the metal oxide overlayers on the bias dependencies of $n$ and $t_{50\%}$ observed in Figures 4 and 5 clearly correlates with the device performance characteristics shown in Figure 6 and Table 2. The $Al_2O_3$ overlayer coated film exhibit not only the smallest acceleration in $t_{50\%}$ under negative biases, devices fabricated from these coated films also exhibit the smallest dark current, and the correspondingly the highest $V_{oc}$. In contrast, the $SiO_2$ overlayer results in an acceleration of recombination dynamics at negative biases, an increased dark current, and correspondingly a lower $V_{oc}$.

It follows from the discussion above that the differences in device performance for the different metal oxide overlayers derives from the influence of these overlayers upon the bias dependence of the film electron density, $n(V)$. This influence can be readily rationalized in terms of differences in acid/base properties of the overlayers. The conduction band energetics of nanocrystalline $TiO_2$ have been shown to exhibit a Nernstein dependence upon electrolyte pH, attributed to protonation/deprotonation of surface oxygen moieties and/or intercalation of protons into the $TiO_2$ nanoparticles.[31] The influence of these protonation processes upon the $TiO_2$ electron density under negative bias may derives from bulk electrostatic effects, or from the introduction of localized sub-bandgap states. With regard to the influence of the overlayer coatings, their influence upon such protonation processes can be determined from consideration of pzc values (the pH values for zero surface charge) for the different metal oxides as indicated in Table 1. An excellent correlation is observed between these pzc values and dependence of the electron densities under negative bias upon the metal oxide overlayers. $Al_2O_3$ has a high pzc (i.e., is basic), indicating that it will tend to deprotonate the $TiO_2$ film, consistent with the relatively low electron densities observed for this film under negative bias. This effect compliments the blocking layer function of this overlayer, resulting in the observed improvement in cell performance. In contrast, $SiO_2$ has a low pzc (i.e., is acidic), resulting in a net protonation of the $TiO_2$, consistent with the higher electron density observed with this overlayer. As a consequence, for high cell voltages, the $SiO_2$ overlayer, despite its insulating function, actually results in an enhancement of recombination losses and, therefore, a lower cell open circuit voltage. Following these observations, it can be concluded that optimum device performance will be achieved with basic metal oxide blocking layers (high pzc's). Studies of alternative high pzc metal oxides, such as MgO, are currently ongoing.

$SiO_2$, $Al_2O_3$, and $ZrO_2$ overlayers resulted in an enhancement in $I_{sc}$ of the DSSC, as indicated in Table 2. This enhancement is most remarked for thicker devices, with devices fabricated from 8 mm $TiO_2$ exhibiting enhancements of $I_{sc}$ by up to 30%, whereas $I_{sc}$ for devices fabricated from 4 mm were largely unaffected by the presence or absence of the overlayer. This effect of film thickness can be readily understood in terms of the relative importance of recombination losses in the devices under short circuit conditions. In a thinner film, electron transport to the $SnO_2$ underlayer is relatively easy, minimizing recombination losses at $I_{sc}$. However for the thicker films, electron transport must proceed further through the film, resulting in higher electron densities in the film at short circuit and therefore more significant recombination losses. Consistent with this interpretation we note that, in contrast to the enhancement in $V_{oc}$, which was found to be highly reproducible, the enhancement in $I_{sc}$ was less reproducible and appeared to be dependent upon the details of the fabrication of the $TiO_2$ film.

Several studies have previously reported that treatment of nanocrystalline $TiO_2$ with $TiCl_4$ solutions results in a significant improvement in device performance.[32] This treatment typically results in a significant improvement in $I_{sc}$, partially offset by a small reduction in $V_{oc}$. The improvement in device performance has been variously attributed to increased film thickness, increased light scattering, increased dye adsorption and necking growth during postannealing leading to improved electron transport.[33−35] We have compared the results we report herein for the $Al_2O_3$, $SiO_2$, and $ZrO_2$ coatings with results we obtain for $TiCl_4$ treatment of the films. $TiO_2$ films were dipped in 0.15 M $TiCl_4$ in 2-propanol for 10 min followed by sintering at 450 °C. Characterization of the resulting films yielded data qualitatively similar to those reported here for $SiO_2$ coated $TiO_2$ films, namely a retardation of the recombination dynamics in the absence of applied bias, an enhanced sensitivity of the recombination dynamics to negatively applied bias, an enhanced electron density in the film under negative applied bias, higher $I_{sc}$ and lower $V_{oc.}$ These results will be presented in full elsewhere. These observations do however suggest that the $TiCl_4$ treatment of nanocrystalline $TiO_2$ films results in a film coating functionally similar to a $SiO_2$ overlayer, namely a coating which is an insulating layer for electron transfer but which increases the electron density in the film under negative bias. The increase in electron density under negative bias is consistent with the acidic nature of $TiCl_4$. It therefore appears possible that the improvement in $I_{sc}$ widely observed with the use of this film treatment may derive, at least in part, from a retardation of interfacial recombination process due to the formation by this treatment of an interfacial blocking layer. This conclusion is consistent with previous observations that the $TiCl_4$ treatment is most effective for improving the efficiency of relatively inefficient devices, with minimal effect on efficient devices in which electron transport through the $TiO_2$ film is already optimized, thereby preventing significant recombination losses at short circuit conditions.[32,35]

(30) Nelson, J.; Haque, S. A.; Klug, D. R.; Durrant, J. R. *Phys. Rev. B: Condens. Matter Materials Phys.* **2001**, *63*, 205 321−205 329.
(31) Rothenberger, G.; Fitzmaurice, D.; Grätzel, M. *J. Phys. Chem.* **1992**, *96*, 5983−5986.
(32) Zhang, D.; Ito, S.; Wada, Y.; Kitamura, T.; Yanagida, S. *Chem. Lett.* **2001**, 1042−1043.
(33) Kambe, S.; Nakade, S.; Wada, Y.; Kitamura, T.; Yanagida, S. *J. Mater. Chem* **2002**, 723−728.
(34) Yin, H.; Wada, Y.; Kitamura, T.; Sumida, T.; Hasegawa, Y.; Yanagida, S. *J. Mater. Chem* **2002**, 378−383.

**Acknowledgment.** The authors are pleased to acknowledge the contribution of Ms. Gabrielle Ehret for the excellent HRTEM measurements at IPCMS-GSI in Strasbourg, Mr. Karol Ksenkiw for the discussion and measurement of XPS data at Imperial College, Johnson Matthey Ltd. for supply of the sensitizer dye, Paul O'Brien for helpful discussions and the EPSRC, Leverhulme Trust and European Union (Contract No. ENK6-CT-2001-00560 Nanomax and Marie Curie Fellowship Contract No. HPMF-CT-2002-01744) for financial support.

JA027945W

(35) Park, N. G.; Schlichthoerl, G.; Van de Lagemaat, J.; Cheong, H. M.; Mascarenhas, A.; Frank, A. J. *J. Phys. Chem. B* **1999**, *103*, 3308−3314.